Smart Structures and Systems, *Vol. 30, No. 4 (2022) 397-410*
https://doi.org/10.12989/sss.2022.30.4.397

Bolt looseness detection and localization using time reversal signal and neural network techniques

Yuanfeng Duan [1,2a], Xiaodong Sui [1,3b], Zhifeng Tang*[4] and Chungbang Yun [1c]

[1] *College of Civil Engineering and Architecture, Zhejiang University, China*
[2] *The Architectural Design and Research Institute of Zhejiang University Co., Ltd., China*
[3] *Center for Balance Architecture, Zhejiang University, China*
[4] *Institute of Advanced Digital Technologies and Instrumentation, Zhejiang University, China*

(*Received March 10, 2022, Revised June 14, 2022, Accepted July 21, 2022*)

Abstract. It is essential to monitor the working conditions of bolt-connected joints, which are widely used in various kinds of steel structures. The looseness of bolts may directly affect the stability and safety of the entire structure. In this study, a guided wave-based method for bolt looseness detection and localization is presented for a joint structure with multiple bolts. SH waves generated and received by a small number (two pairs) of magnetostrictive transducers were used. The bolt looseness index was proposed based on the changes in the reconstructed responses excited by the time reversal signals of the measured unit impulse responses. The damage locations and local damage severities were estimated using the damage indices from several wave propagation paths. The back propagation neural network (BPNN) technique was employed to identify the local damages. Numerical and experimental studies were conducted on a lap joint with eight bolts. The results show that the total damage severity can be successfully detected under the effect of external force and measurement noise. The local damage severity can be estimated reasonably for the experimental data using the BPNN constructed by the training patterns generated from the finite element simulations.

Keywords: bolt looseness detection and localization; BP neural network; guided SH waves; joint with multiple bolts; reconstructed responses; time reversal signal

1. Introduction

Bolt connection is a common assembly form widely used in mechanical, aerospace and civil engineering industries. Under the action of environmental factors such as vibration or corrosion, bolts may easily get loosened, which may affect the overall stability of the structure and cause severe accidents (Pai *et al*. 2002, Yang *et al*. 2015, Pnevmatikos *et al*. 2016). Therefore, development of effective methods for bolt looseness detection has attracted considerable attention from researchers.

Bolt looseness detection has traditionally relied on strain gauge and torque wrench techniques (Ahmadian and Jalali 2007, Nikravesh and Goudarzi 2017). However, it is often not feasible to attach strain gauges on bolts because of their sizes and locations. The accuracy of the torque wrench method is very much influenced by the friction between the bolt threads and nuts, and the method requires manual operation. Thus, various structural health monitoring (SHM) methods have been proposed and implemented to estimate bolt torque conditions. The vibration-based damage assessment method was proposed by analyzing the changes in the structural dynamic properties, such as the transmittance function and power spectral density (Caccese *et al*. 2004, Razi *et al*. 2013). Zhang *et al*. (2017) extended the vibroacoustic method by combining the low-frequency mechanical vibration and high-frequency acoustic waves. A laser-based vibration measurement method was proposed to improve the quality and reliability of the test methodology (Huda *et al*. 2013). Liang *et al*. (1997) developed the theory of the impedance measurement method and applied it to SHM. Park *et al*. (2005) conducted an experimental study on the steel bridge components using the piezoelectric transducer and electromechanical impedance methods. Min *et al*. (2012) introduced a neural network-based optimal frequency range selection method to fully analyze the impedance information and improve the test accuracy. Furthermore, Chen *et al*. (2020) proposed a smart washer to achieved damage localization by embedding PZT into two flat metal rings. Recently, machine vision techniques have been widely adopted owing to the rapid progress in instrument development (Cha *et al*. 2016, Chung and Sohn 2020). Localizations and damage severities are generally detected by extracting special features from the visual images; however, the accuracy greatly depends on the quality of the pictures. The guided wave method is one of the most attractive nondestructive testing techniques owning to single-point excitation, long sensing range, and high-efficiency detection (Beena *et al*. 2017). It has been

*Corresponding author, Professor,
E-mail: tangzhifeng@zju.edu.cn
[a] Professor, E-mail: ceyfduan@zju.edu.cn
[b] Ph.D. Student, E-mail: 11712067@zju.edu.cn
[c] Professor, E-mail: ycb@zju.edu.cn

ISSN: 1738-1584 (Print), 1738-1991 (Online)

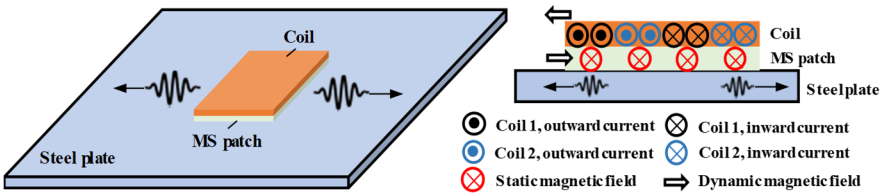

Fig. 1 Diagram of the MS transducer

widely studied and adopted in real engineering applications for local damage detection on pipes, steel plates, rails, and cables (Hayashi and Murase 2005, Moustakidis *et al*. 2014, Kamas *et al*. 2015, Tang *et al*. 2021).

The pitch-catch typed guided wave method was commonly used for damage detection of bolt-connected structures, where the guided wave generated from one side of the structure was transmitted through the lap joints and received by the transducer on the other side. The received signal was directly affected by the real contact conditions between the two plates at the joint. Thus, a quantitative relationship can be constructed between the bolt torque (or tension) and specific features of the received guided wave signals. Jhang *et al*. (2006) estimated the bolt torque by measuring the wave velocity variation. However, the wave velocity change was small, and transducers were not easy to be installed on the cross-section of the bolt thread. High-resolution data acquisition equipment was required to guarantee measurement accuracy. The energy-based guided wave method was also presented by calculating the energy of the directly arrival wave packet (Park *et al*. 2006). However, the bolt looseness was undetectable when the damage severity was small. Several nonlinear acoustic methods were developed by taking advantage of the breathing motion at the plate interface (Amerini and Meo 2010, Baghalian *et al*. 2018). A contact acoustic nonlinear index was proposed using the high-order harmonics and spectral sidebands, but the results are not quite consistent. The above review of the current guided wave-based bolt looseness detection methods indicated that most studies focused on the single bolt condition (Pai and Hess 2002, Jhang *et al*. 2006, Fasel *et al*. 2009, Amerini and Meo 2010, Huda *et al*. 2013, Zhang *et al*. 2017, Chen *et al*. 2020), which is not used in real structures. Furthermore, studies on the complicated multi-bolt conditions (Park *et al*. 2006, Baghalian *et al*. 2018, Zhang *et al*. 2019) only gave the total damage severity information and could not determine the damage locations and local damage severities. Therefore, a time reversal signal (TRS)-based guided wave method (Fink *et al*. 2000, Parvasi *et al*. 2016) is employed in this study to detect and locate the looseness in multiple bolts using small numbers of transducers. The degree of looseness of the bolt group can be analyzed based on the peak amplitude of the reconstructed signal excited by TRS. The local damage severities and damage locations can be determined by inputting the peak amplitude information from various wave propagation paths into the back propagation neural network (BPNN).

There are three types of guided waves in the plate structure: symmetric Lamb wave, antisymmetric Lamb wave, and SH wave. SH wave is an in-plane wave with the vibration direction parallel to the surface, whereas the vibration directions of the Lamb waves are out-of-plane. Zhang *et al*. (2021) carried out experimental tests for bolt looseness detection using SH wave. It has been found that the SH wave was less affected by the surface medium, such as rain, oil, or paint coating, on the wave propagation paths. Moreover, the wave energy attenuation is much more severe in the Lamb wave when it passes through a liquid interface, making it difficult to be used in such situations. Generally, SH waves can be generated through piezoelectric and magnetostrictive (MS) transducers. Although various configurations of the PZT array have been presented for exciting and receiving SH waves (Kubrusly and Dixon 2021, Miao and Li 2021), the energy conversion efficiency is sensitively influenced by the temperature (Gianesini *et al*. 2020) and bonding conditions between transducers and test specimen (Na and Lee 2012). Fig. 1 shows a schematic of the MS transducer for generating SH waves developed at Zhejiang University (Zhang *et al*. 2021). It consists of a pre-magnetized MS (iron-cobalt) patch to provide the static magnetic field and a coil unit to provide the dynamic magnetic field. The MS patch is very thin, and it can be bonded to the steel plate using an epoxy coupling agent. The coil is attached to the MS patch. MS transducers generally show great performance under a wider range of temperatures than PZT transducers (Su *et al*. 2006), and provide more robust performance under the rain/oil-surface environments (Tang *et al*. 2021). Therefore, MS transducer-generated SH waves were implemented for bolt looseness detection in this study.

A guided wave-based method for bolt looseness detection and localization is presented for a joint structure with multiple bolts. SH waves generated and received by a small number (two pairs) of magnetostrictive transducers were used. The remainder of the paper is organized as follows. In Section 2, the dispersion properties of the plate are investigated, and a TRS-BPNN-based method for bolt looseness detection and localization is introduced. In Section 3, numerical simulation analysis on an example lap joint is conducted to validate the proposed method. In Section 4, experimental tests are performed, and the damage locations and local damage severities are estimated using BPNN trained by the patterns from finite element simulations. Finally, Section 5 presents the conclusions.

2. Damage detection using SH wave and TRS-BPNN method

2.1 Dispersion property analysis of plate structure

First, the dispersion properties were analyzed for the

Table 1 Basic parameters of the steel plate

Size (mm)	Young's modulus (GPa)	Poisson ratio	Density (kg/m^3)
1300 × 250 × 8	210	0.28	7850

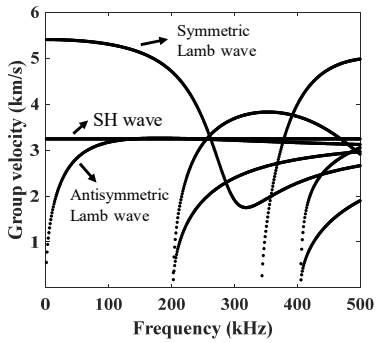

Fig. 2 Dispersion curve of the steel plate

plate structure used in the example study. Table 1 shows the basic parameters of the steel plate. The governing equations of the SH waves can be derived according to the Helmholtz principle (Fan and Lowe 2009). The group velocity dispersion curve was obtained using the semi-analytical finite element method (Tang *et al*. 2021), as shown in Fig. 2. It has been observed that the SH mode guided wave is non-dispersive in the low-frequency range, whose group velocity does not change with the excitation frequency. In this study, the excitation frequency was selected as 80 kHz for bolt looseness detection considering available MS transducers (Tang *et al*. 2021). Three modes, including symmetric (S) and antisymmetric (A) Lamb waves and SH wave, exist under the excitation frequency of 80 kHz. However, the existence of certain mode in the received signal depends on the excitation type. SH wave was selectively generated using the MS transducer. The direction of the static magnetic field by pre-magnetizing on the MS patch was orthogonal to the direction of the dynamic magnetic field provided by the coil unit as in Fig. 1. Under this configuration, an in-plane shear deformation will occur on the MS patch and SH wave can be generated. But the vibration direction of S and A Lamb waves are out-of-plane, thus these modes cannot be generated.

2.2 TRS method for total bolt looseness detection

The real contact area between two steel plates at a lap joint is smaller than its nominal contact area owing to the rough surface, which varies with the tension applied on the bolts. The sinusoidal micro-contact model and classical Hertz contact theory have been widely used to calculate the real contact area under a prescribed load (Biwa *et al*. 2004). Ultrasonic guided waves propagated through the lap joint reflect the actual contact condition on the interface. Therefore, the bolt tension condition may be estimated by analyzing the characteristics of the transmitted waves.

In this study, the TRS-method (Parvasi *et al*. 2016) is used to analyze the transmitted waves. The time reversal of the measured impulse response is used as a new excitation to obtain a reconstructed response. The TRS-method is based on the worst excitation theory, which may drive the system to the maximum response at t_0 under the condition of a same mean square intensity of the excitation (Drenick *et al*. 1980). For a lap joint connected by multiple bolts shown in Fig. 3, two transducers on the left steel plate work as the actuators, whereas the other two on the right act as the receivers. For an excitation $f_i(t)$ applied to an actuator A_i, the received response $y_{ji}(t)$ at a receiver R_j can be expressed as follows

$$y_{ji}(t) = \int_0^t f_i(\tau) h_{ji}(t-\tau) d\tau \tag{1}$$

where $h_{ji}(t)$ is the unit impulse response function at R_j for a unit impulse $f_i(t) = \delta(t)$ at A_i. The overall amplitudes of $h_{ji}(t)$ and $y_{ji}(t)$ will be reduced with the reduction of the contact area and bolt tension condition at the joint.

TRS is defined as the time reversal of the measured unit impulse response $y_{ji}(t)$ at a time instance t_0 as follows

$$y_{ji}(t_0 - t) = h_{ji}(t_0 - t) \tag{2}$$

If TRS $y_{ji}(t_0\text{-}t)$ is retransmitted as an excitation at A_i, the reconstructed response signal $Y_{ji}(t)$ at R_j can be obtained as follows

$$Y_{ji}(t) = \int_0^t h_{ji}(t_0 - \tau) h_{ji}(t-\tau) d\tau \tag{3}$$

Obviously, the maximum value of $Y_{ji}(t)$ is obtained at $t = t_0$, which is given by

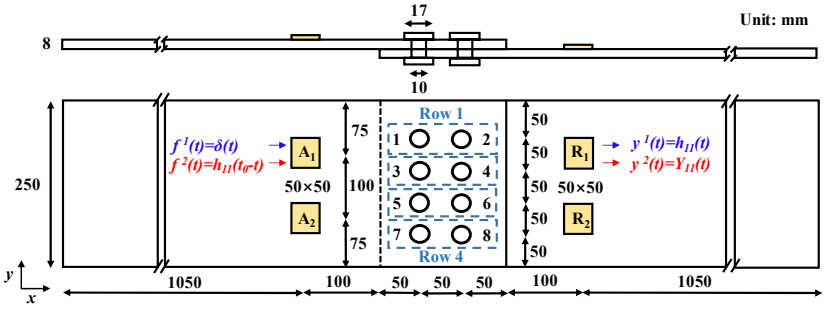

Fig. 3 Layout of the bolt connected structure

$$Y_{ji}(t_0) = \int_0^{t_0} h_{ji}^2(t_0 - \tau)d\tau \quad (4)$$

It is to be noted that the TRS was applied to the actuator (A_1, A_2) and the reconstructed response was measured at the receiver (R_1, R_2), whereas the TRS was introduced to the receiver in the paper by Parvasi *et al.* (2016). Two methods will give the same results of $Y_{ji}(t)$ owing to the reciprocal theorem for the linear system: $h_{ji}(t) = h_{ij}(t)$. However, the present scheme is more convenient, because there is no need to exchange the actuator and receiver in the case with two different sensor types.

The above reconstructed responses, $Y_{ji}(t)$ and $Y_{ji}(t_0)$, shall vary with the bolt tension condition at the joint. In this study, a quantitative damage index (DI_{ji}) is proposed to estimate the bolt tension based on the change in $Y_{ji}(t_0)$, as shown in Eq. (5). DI_{ji} for the *ji-th* pair of the pitch-catch test is defined based on the amplitude ratio between the values of $Y_{ji}(t_0)$ in the damaged and intact cases ($Y_{ji}^d(t_0)$ and $Y_{ji}^0(t_0)$), which is getting larger with increasing damage severity.

$$DI_{ji} = 1 - \frac{Y_{ji}^d(t_0)}{Y_{ji}^0(t_0)} = 1 - \frac{\int_0^t h_{ji,d}^2(t_0 - \tau)d\tau}{\int_0^t h_{ji,0}^2(t_0 - \tau)d\tau} \quad (5)$$

where $h_{ji,d}(t)$ and $h_{ji,0}(t)$ are the impulse response functions under the damaged and intact conditions, respectively.

Four DI_{ji} can be obtained for a bolt-connected joint in Fig. 3 corresponding to four wave paths in the pitch-catch tests (A_1-R_1, A_1-R_2, A_2-R_1, and A_2-R_2) by two actuators and two receivers. The total damage severity of the joint can be evaluated as an average of four DI_{ji} as

$$DI_{overall} = \frac{1}{4}\sum_j^2 \sum_i^2 DI_{ji} \quad (6)$$

2.3 TRS-BPNN method for local bolt looseness detection

After obtaining the total damage severity, the general damage location may be determined using the relationships between four DI_{ji} and local bolt loose conditions. However, it is not easy to find a universal law in DI_{ji} to locate the damages, as described in Section 3.3. Thus, this paper presents a TRS-BPNN-based local bolt looseness detection method using the DI_{ji} obtained from the pitch-catch tests as the input to the BPNN. BPNN is a multi-layered feedforward network trained by the back propagation of error, which has been widely used in SHM and condition assessment. Many researchers used the dataset with various damage cases from experiments to train and test the BPNN (Lopes *et al.* 2000, Min *et al.* 2012). However, it is very difficult to generate a sufficient number of training patterns for various damage severities through experiments in practice. Thus, it is essential to use sample patterns from the simulation analysis to train the BPNN, which will be used to estimate the local damage severity on the experimental data. A finite element model (FEM) was constructed for the wave propagation analysis on the joint structure to generate various training patterns, as described in Section 3.1.

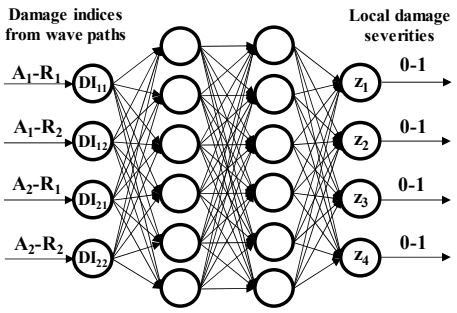

Fig. 4 Diagram of the BP neural network

For a lap joint shown in Fig. 3, a four-layered BP neural network was established as shown in Fig. 4. The input layer consists of four nodes for four DI_{ji} values of four different wave paths. It is generally difficult to estimate the local damage for each of the eight bolts using only four input data. Thus, the entire bolt group was divided into four subgroups (four rows), and four output nodes were assigned to the output layer with the value of the local damage severity (bolt tension loss rate) z_i between 0 (intact) and 1 for each row. For example, the output $\{z\}$ for a case with one bolt totally loose at Row 2 is labeled as $\{0, 0.5, 0, 0\}$.

3. Numerical simulation study

3.1 Finite element model and analysis procedure

A three-dimensional FEM was constructed using ABAQUS to generate training patterns for the BPNN, as shown in Fig. 5. The geometric and material properties of the steel plates were the same as those in Table 1. Bolts and MS transducers were arranged, as shown in Fig. 3. The prescribed tension in each bolt was taken as 23000 kN, which is 70% of the allowable value as in the standard (GB 50205 2020). The maximum mesh sizes are 5 and 1.5 mm for the plates and bolts, respectively. The number of the linear solid hexahedral elements with eight nodes is 72211. Contact conditions between two plates at the lap joint were simulated using the hard contact in the normal direction and friction condition in the tangential directions with a friction coefficient of 0.3 (Parvasi *et al.* 2016). The numerical analysis process consists of a static analysis to obtain the pressure in the contact area under bolts tension and a dynamic analysis for the guided wave propagation.

In the first static analysis process, the bolt load was gradually applied until it reached the preset tension. The bolt was simulated by two bolt nuts and a bolt thread.

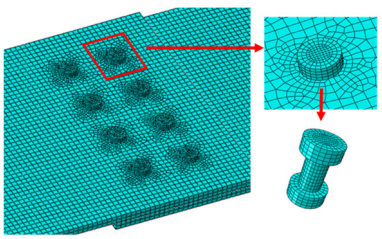

Fig. 5 Meshes of the finite element model

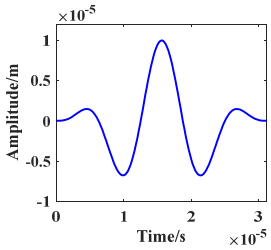

(a) Excitation signal at A_1

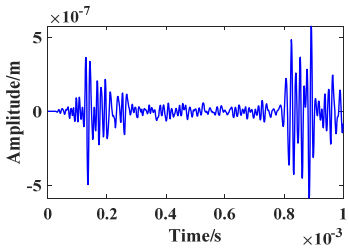

(b) Received signal $y_{11}(t)$ at R_1

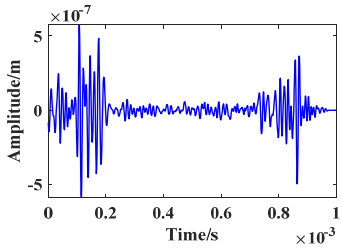

(c) Time reversed signal $y_{11}(t_0 - t)$

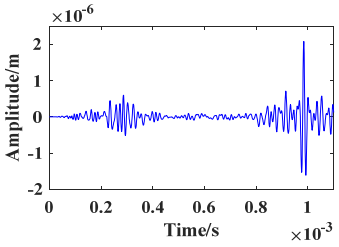

(d) Reconstructed signal $Y_{11}(t)$ at R_1

Fig. 6 FEM simulation results for the TRS method

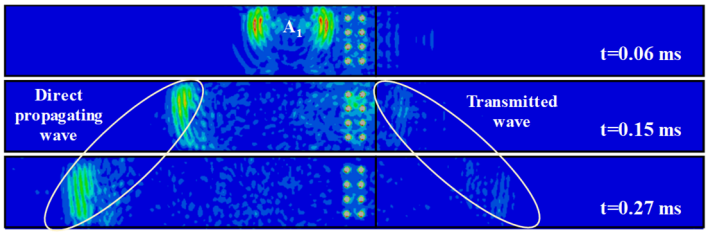

Fig. 7 Energy distribution of the guided SH waves during the wave propagation

The type of Bolt Load in ABAQUS was adopted to apply the bolt tension. Different damage cases were simulated by changing the bolt load in this process. Dynamic analysis was conducted with the pressures in all finite elements on the contact surface obtained from the static analysis. The sampling frequency was taken as 1 MHz. The excitation signal for the SH wave was simulated by applying the nodal displacement on the actuating transducers along the *y* axis (horizontal and transverse) in Fig. 3.

The TRS method was originally developed based on the unit impulse excitation (Parvasi *et al*. 2016). However, the frequency range of the unit impulse is very wide, and the MS transducer works well around its central frequency range. Thus, a 2.5-cycle sinusoidal tone-burst signal modulated by the Hanning window with a central frequency of 80 kHz (Fig. 6(a)) was used as an approximation. There are two steps in the dynamic analysis process using TRS. At the first step, a tone-burst signal shown in Fig. 6(a) was applied at an actuator A_i on the left plate. The response was measured at a receiver R_j on the right plate for a duration of 1 ms, as in Fig. 6(b). At the second step, the received time signal was reversed at t_0 = 1 ms (Fig. 6(c)), and retransmitted to A_i as an excitation. Next, the reconstructed signal $Y_{ji}(t)$ was obtained at R_j, as shown in Fig. 6(d). The peak amplitude appeared near t = 1 ms in the reconstructed signal, which would be used to calculate the damage index DI_{ji} using Eq. (5). The peak amplitude did not appear exactly at 1 ms because the peak excitation was not exactly at t = 0, as shown in Fig. 6(a). Fig. 7 demonstrates the wave propagation process for the first step. At 0.06 ms, the SH waves initiated at A_1 propagated into two opposite directions. The right part of the SH wave has passed through the contact region at 0.15 ms and continues propagating on the right steel plate. It could be found that the transmitted wave energy through the lap joint is much smaller than that of the directly propagating waves to the left at 0.27 ms.

3.2 TRS-based total damage severity estimation

3.2.1 Selection of excitation type

The performance of the two types of excitation signals (unit impulse and 2.5-cycle tone-burst) were investigated, as shown in Figs. 8 and 9. It has been found that the peak amplitudes of the reconstructed responses decreased gradually with the increase in damage severity by both excitation signals, as shown in Fig. 8. The reconstructed response $Y_{11}(t)$ using the tone-burst excitation was distinct near t = 1 ms. The overall damage index ($DI_{overall}$) was evaluated using Eq. (6) for various damage severities. Fig. 9 shows the results against the total tension loss rate. The total tension loss rate represents the total bolt looseness severity in the eight bolts. The damage level was gradually increased with the number of the totally loosed bolt from 1

(a) Unit impulse (b) 2.5-cycle tone-burst signal

Fig. 8 Reconstructed signals under different damage severities

(a) Unit impulse (b) 2.5-cycle tone-burst signal

Fig. 9 Total damage severity estimation results

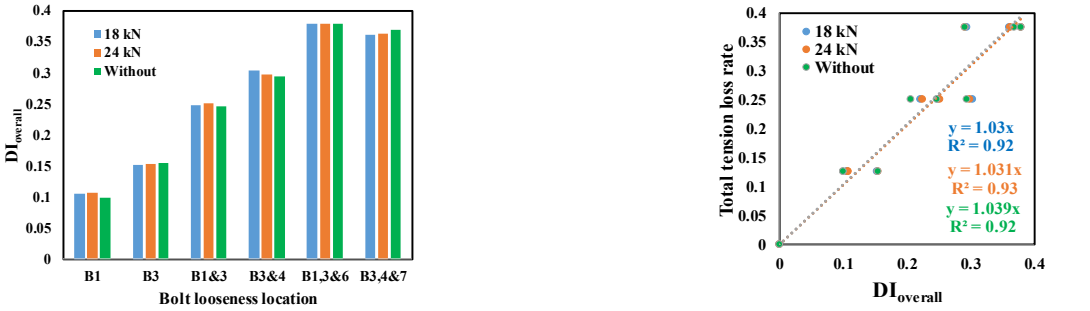

(a) Changes of $DI_{overall}$ under external force (b) Regression curves under external force

Fig. 10 Total damage severity estimation considering the external force

to 6, so the total tension loss rate varies from 1/8 to 6/8 with the interval of 1/8. Several scenarios with different damage locations were calculated for each damage level. Linear regression curve was obtained as $y = 1.222x$ ($R^2 = 0.98$) for the unit impulse, and $y = 1.084x$ ($R^2 = 0.97$) for tone-burst signal, where x is the overall damage index and y is the total tension loss rate. Excellent linear regression relationships were found with similar regression coefficients and large values of R^2 under two kinds of excitations. Thus, the tone-burst signal with a central frequency of 80 kHz (Fig. 6(a)) was adopted as the excitation signal in the FEM simulation and experimental tests to estimate the tension loss.

3.2.2 Influence of the external force on plates

Bolt-connected joints are usually subjected to an external force in the tangential direction during the operation period. Thus, it is essential to investigate the influence of the external force on the TRS method. The shear capacity of a single bolt was calculated as 6.21 kN in this example. Two levels of axial force with 18 and 24 kN were applied along the x-axis of the plate in the static analysis process. Fig. 10(a) shows the comparison of $DI_{overall}$ under several damage scenarios, indicating that small changes occur due to the external forces. The total damage severity rate under the external force was taken to be less than 0.4, considering the shear capacity of the bolt group. Three linear regression curves for three levels of external forces were almost the same, as shown in Fig. 10(b), indicating a small effect of the external force on the TRS method.

3.2.3 Effect of measurement noise

The measurement noise effect was also investigated by adding white noise to the TRS to examine the influence on

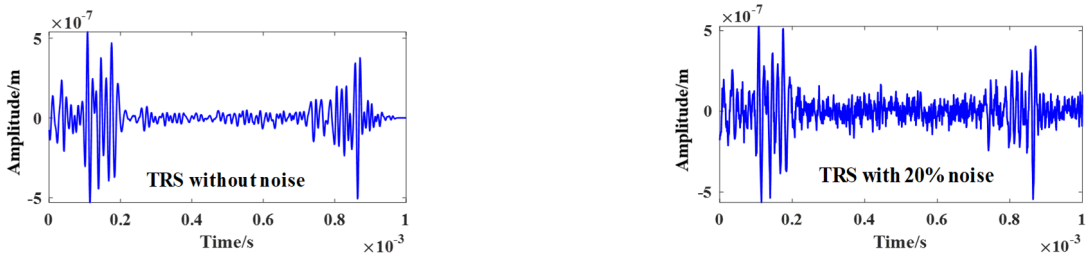

Fig. 11 TRS without and with noise

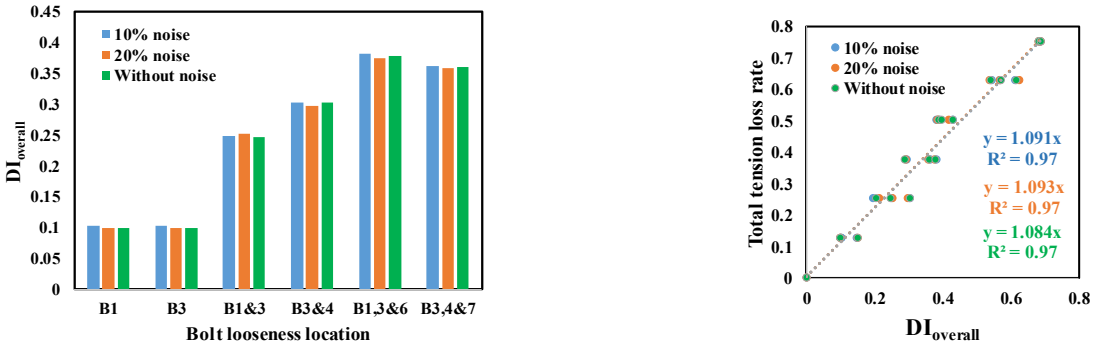

(a) Changes of $DI_{overall}$ under noise effect (b) Regression curves under noise effect

Fig. 12 Total damage severity estimation considering the noise effect

the TRS method. The power ratio between the noise and signal was taken as 10% and 20% in RMS level, corresponding to the signal-to-noise ratios (SNRs) 10 and 7 dB, as in Eq. (7). Fig. 11 shows the TRS with 20% noise in RMS. The reconstructed signals and overall damage indices were obtained for different damage severities, and the changes in the overall damage index were found to be very small under the noise effect, as shown in Fig. 12(a). Fig. 12(b) shows that the three regression curves under the three noise levels were practically the same, indicating that the proposed TRS method is insensitive to the measurement noise.

$$\mathrm{SNR}_{db} = 10log\frac{RMS(Signal)}{RMS(Noise)} \tag{7}$$

3.2.4 Total tension loss rate in early damage stage

The regression curve obtained from the simulation results is used to estimate the total tension loss rate of the bolt group. To evaluate the performance of the proposed method, 486 training samples, as described in Section 3.3, were used to obtain the regression curve. The total damage severities of the 486 cases were less than 0.4, which represent the early damage stage of the lap joint. A new regression curve was obtained as $y = 1.219x$ ($R^2 = 0.75$) (Fig. 13), which has a slightly larger linear coefficient (1.219) than the one (1.084) in the regression curve for a wide damage range (0-0.8) shown in Fig. 9(b). The total damage severities were estimated using the new regression curve for the early damage state. The estimation error obtained using Eq. (8) was 6.2% for the 96 testing samples in Section 3.3, indicating the excellent performance of the TRS method for total tension loss rate estimation.

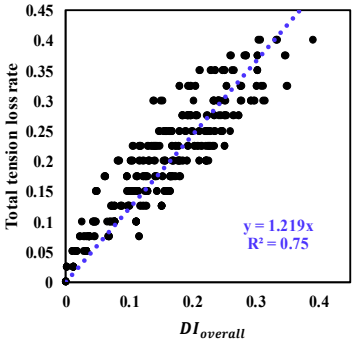

Fig. 13 Total damage severity vs $DI_{overall}$ in the early damage stage

$$Error^{total} = \sqrt{\sum_{j=1}^{96}\left(F_j^{real} - F_j^{est}\right)^2 \Big/ \sum_{j=1}^{96}\left(1 - F_j^{real}\right)^2} \tag{8}$$

where F_j^{est} is the estimated total tension loss rate using the new regression curve (Fig. 13) through FEM simulation for the jth damaged case; F_j^{real} is the real damage severity for the jth case.

The total damage detection results were compared with those obtained using the wave energy method incorporating the wavelet transform proposed by Park *et al.* (2006). The wave energy-based damage indices were defined in Eqs. (9) and (10). They were calculated using the first-arrival wave packet under the intact $(y_{ji}^0(t_0))$ and damaged conditions $(y_{ji}^d(t_0))$ in the period $[t_s, t_f]$. Here t_s is the time when the SH wave reaches the receiver, and the interval between t_s and t_f is the time period of the excitation signal (0.036 ms);

t_s is determined from the distance between the actuator and receiver and the group velocity of SH wave obtained from the dispersion curve in Fig. 2, which was 0.106 and 0.109 ms for the wave paths A_1-R_1 and A_1-R_2, respectively.

$$DI_{ji}^{WE} = \sqrt{\sum_{t_s}^{t_f}[y_{ji}^0(t) - y_{ji}^d(t)]^2 / \sum_{t_s}^{t_f}[y_{ji}^0(t)]^2} \quad (9)$$

$$DI_{overall}^{WE} = \frac{1}{4}\sum_j^2 \sum_i^2 DI_{ji}^{WE} \quad (10)$$

Fig. 14 shows the regression curve for total damage estimation using the wave energy-based method. The linear coefficient (1.226) is almost same to that obtained by the proposed TRS-based method, however the R^2 value (0.4) becomes considerably poorer. The estimated error for the total damage severity was 12.5% for the 96 test samples, indicating that the proposed TRS method performs better than the wave energy method.

3.3 TRS-BPNN based local damage detection

Fig. 15 shows the damage indices DI_{ji} obtained from *ji-th* pairs of the pitch-catch tests for different damage conditions, which may be used to estimate the damage locations. It can be predicted that bolt looseness occurs in the upper rows (B1-B4 in Fig. 3) by detecting that DI_{11} for the wave path A_1-R_1 is consistently larger than DI_{22} for the wave path A_2-R_2. However, it is difficult to find laws to exactly locate the loose bolts among the four upper bolts.

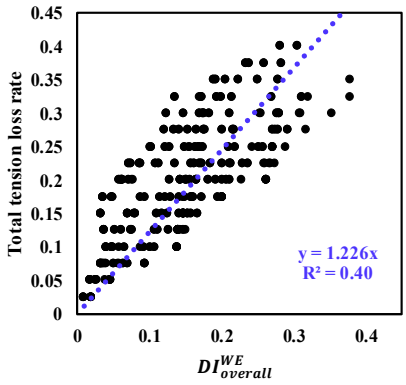

Fig. 14 Total damage severity vs $DI_{overall}^{WE}$ by the wave energy-based method

Therefore, this study proposed the TRS-BPNN method using 4 DI_{ji} values as the input of the BPNN to better locate the damage and predict the local damage severity using a set of limited numbers of transducers for the joint with multiple bolts. The output of BPNN and the label of each sample was a vector with four elements representing the damage locations and local damage severities of the four rows. Then, numerical simulation was conducted for various damage scenarios to generate the training and testing patterns. In this example, damage detection was carried out for early bolt looseness conditions. Thus, the damage was assumed to occur at most in two among four rows of the bolts, producing six different combinations of two damage locations (C_4^2). For the training patterns, the local damage severity for each row was selected as nine levels in the range of 0-0.8 with an equal interval of 0.1. Consequently, the number of the training samples was 486 (6 × 9 × 9). More training patterns may be used in a real application to improve damage prediction accuracy. For the testing patterns, four damage levels of 0.25, 0.35, 0.45, and 0.65 were considered for each row. Thus, the number of test sample cases was 96 (6 × 4 × 4). It is to be noted that the purpose of this paper is not to identify the looseness of each bolt, which may not be practical to the joints with multiple bolts as in large civil engineering structures. Instead, the bolts were divided into 4 subgroups to investigate the effectiveness of the proposed method in the local-level damage identification. The damage severities for the two bolts in each subgroup were assumed to be the same for individual damage case. Different damage severities in a subgroup may lead to different wave transmission, which may be investigated in the further studies.

The BPNN model was built using the machine learning toolbox in Matlab, which has been widely used by many researchers. The training and testing processes were conducted on the laptop (Lenovo Ideapad 720 s). The BPNN structure was taken as the one with two hidden layers. The number of nodes in each hidden layer was taken as six through a parametric study described in Table 2, later. The activation function was tansig for the hidden layers, as shown in Fig. 16, and linear connection for the output layer. The number of training patterns was larger than two times of the total number of weights, which satisfies the Vapnik-Chervonenkis dimension theory (Hush and Horne 1993). The Levenberg-Marquardt optimization algorithm was used as the training function with the learning rate of 0.0001. The mean square error was used as the loss function at the output layer. The entire training and testing process took

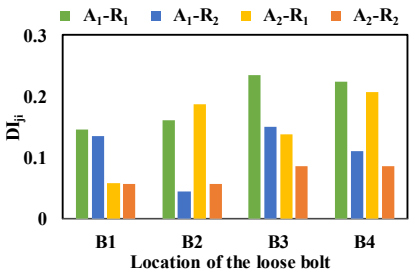

(a) Single damage cases

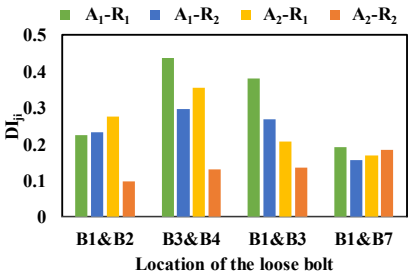

(b) Double damages cases

Fig. 15 DI_{ji} for different damage conditions

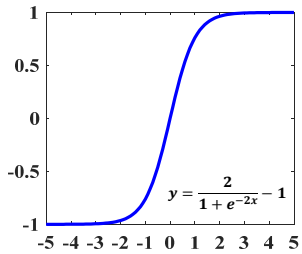

Fig. 16 Activation function: tansig

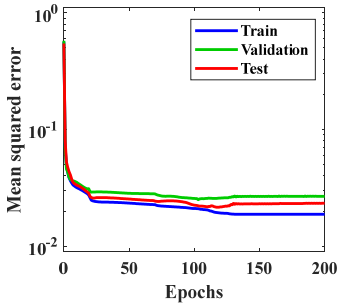

Fig. 17 Loss in the training process

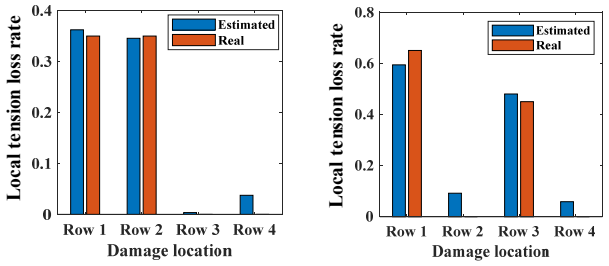

(a) Case 1 (b) Case 2

Fig. 18 Local damage detection results based on FEM simulation

less than 2 s with the training, validation, and testing loss shown in Fig. 17. After training with 200 epochs, the training loss stayed around 0.019, and the validation and testing losses were 0.027 and 0.023, respectively.

Fig. 18 shows two examples of local damage detection results, which indicate the good performance of the proposed TRS-BPNN method. Fig. 19 shows the local damage severity estimation results for each row of 96 testing cases. It can be found that most of the damages were identified, though the estimated values were slightly different from the label values and false alarms with relatively small values occurred in a number of cases. To quantitatively evaluate the local damage severity estimation accuracy, the relative error for the local damage severity prediction was defined in terms of the root mean square of the relative value, as given in Eq. (11).

$$\text{Error}_i^{local} = \sqrt{\sum_{j=1}^{96}(f_{ij} - z_{ij})^2 / \sum_{j=1}^{96}(1 - f_{ij})^2} \quad (11)$$

where z_{ij} is the predicted local damage severity of the ith row for the jth damaged case using the TRS-BPNN method, and f_{ij} is the corresponding label. The relative errors in the local damage severity prediction for Rows 1 to 4 were 0.113, 0.152, 0.136, and 0.104, respectively with an average value of 0.126, as shown in Table 2.

To further examine the damage localization accuracy, three indicators, including precision (P), recall (R), and F1-score (F) were adopted (Zhou 2016). It is assumed that damage exists at a certain row if the output value of BPNN is larger than 0.15. The threshold was determined considering the test damage severity and previous studies on single bolt looseness detection (Parvasi *et al.* 2016). Then, the predicted results were classified into TP (true positive), TN (true negative), FP (false positive), and FN (false negative), respectively. The P, R, and F were defined in Eqs. (12)-(14). P represents the rate of the correctly detected damage, whereas 1-P is the false alarming rate. R represents the rate of the detected damage among all damage cases, while 1-R is the damage missing rate. F combines P and R to show an average damage localization performance of BPNN.

$$P = TP/(TP + FP) \quad (12)$$

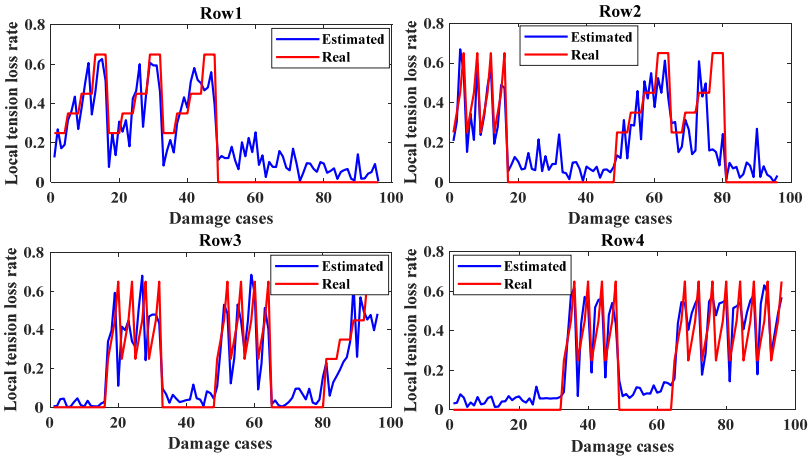

Fig. 19 Local damage severity estimation results based on FEM simulation

Table 2 Local damage detection results for different structures of BPNN

Structure of BPNN	Row	P	R	F	$Error^{local}$
*Two hidden layers [6, 6]	Row 1	0.917	0.863	0.889	0.113
	Row 2	0.896	0.935	0.915	0.152
	Row 3	0.875	0.977	0.923	0.136
	Row 4	0.938	1.000	0.968	0.104
	Average	0.906	0.944	0.924	0.126
Two hidden layers [8, 8]	Row 1	0.833	0.833	0.833	0.131
	Row 2	0.958	0.958	0.958	0.120
	Row 3	0.875	0.955	0.913	0.149
	Row 4	0.917	0.880	0.898	0.130
	Average	0.896	0.907	0.901	0.133
Two hidden layers [10, 10]	Row 1	0.917	0.863	0.889	0.114
	Row 2	0.875	0.933	0.903	0.123
	Row 3	0.917	0.978	0.946	0.133
	Row 4	0.958	0.821	0.885	0.145
	Average	0.917	0.899	0.906	0.129
Three hidden layers [6, 8, 6]	Row 1	0.917	0.815	0.863	0.162
	Row 2	0.896	0.896	0.896	0.129
	Row 3	0.896	0.977	0.935	0.140
	Row 4	1.000	0.842	0.914	0.161
	Average	0.927	0.883	0.902	0.148

*Note: This BPNN structure is used in this study

$$R = TP/(TP + FN) \tag{13}$$

$$F = 2 \times P \times R/(P + R) \tag{14}$$

Table 2 presents the local damage detection results using different BPNN structures. Compared with the other BPNN structures, the proposed structure with two hidden layers and six nodes in each layer achieved better performance with the better accuracy (F value) of 92.4% for damage localization and smaller error (12.6%) for local damage severity estimation. The average false alarming rate (1-P) was 9.4%, whereas the damage missing rate (1-R) was 5.6%.

4. Experimental study

4.1 Experimental setup

Experimental validation was conducted to verify the proposed TRS-BPNN based guided wave method. The material properties and the dimension of the test specimen are the same as those in Table 1 and Fig. 3. Four MS transducers were installed to generate and receive the guided waves, as in Fig. 3. Each MS transducer consists of an iron-cobalt MS patch and a coil. The MS patch was attached to the steel plate through an epoxy coupling agent (LOCTITE E-05CL), and the coil was coupled to the MS patch by adhesive tape. The pitch-catch method was used with two MS transducers on the left plate (A_1, A_2) as actuators and the other two (R_1, R_2) on the other plate as the receivers. The excitation signal generated by the arbitrary signal generator (Rigol DG-1022) was amplified using a power amplifier (AE Techron 7224), then transmitted to the coil. The generated guided waves were received, amplified, and modulated by the data acquisition equipment in Fig. 20(b), developed at Zhejiang University. The sampling frequency was 1 MHz, and a personal laptop was used to control the equipment and store the signals. Besides, a torque wrench was used to adjust the bolt torque. The relationship between the torque T and bolt tension F may be approximately obtained as (GB 50205 2020)

$$T = K \times F \times d \tag{15}$$

where, K is the torque quotient; d is the diameter of the bolt.

4.2 Results for total damage severity estimation

Bolt looseness cases considered in the FEM simulation were tested by experiments, where bolt forces were given in torque. Fig. 21 shows the received signal $y_{11}(t)$ and the single frequency component at the excitation frequency (80 kHz) obtained by wavelet transform, which were compared with the simulated results. The overall shapes of the wave packets received by experiment were similar to the FEM

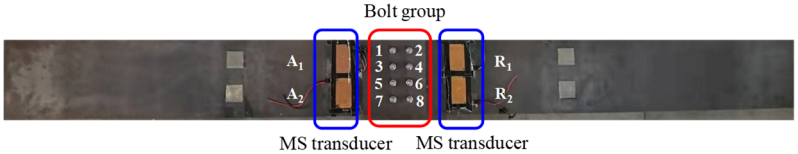

(a) Layout of the test specimen

(b) Data acquisition equipment

(c) Arbitrary signal generator

(d) Power amplifier

Fig. 20 Guided wave inspection system

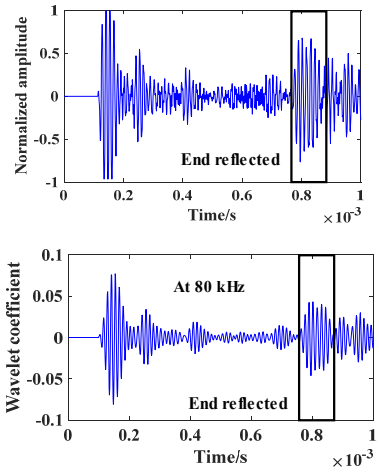

(a) y_{11}(t) and wavelet component at 80 kHz by experiment

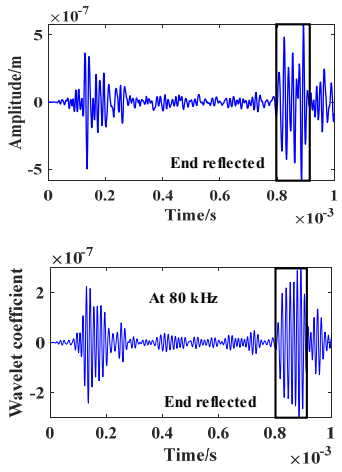

(b) y_{11}(t) and wavelet component at 80 kHz by simulation

Fig. 21 y_{11}(t) by a tone-burst excitation with 80 kHz at the intact case

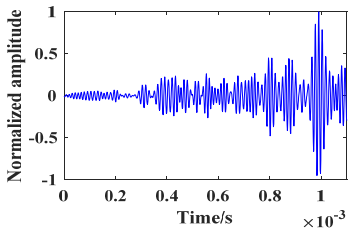

(a) Intact case

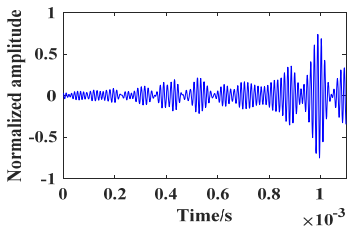

(b) Damaged case: {z} = {0.65, 0, 0.65, 0}

Fig. 22 Reconstructed responses of Y_{11}(t) by experiment

simulation results, though the amplitude of the end reflected wave packet from the experimental result was relatively smaller, which was caused by the larger energy attenuation during the wave propagation process in the experiment. The reconstructed signals of Y_{11}(t) by experimental tests were shown in Fig. 22. The 96 test cases used in the simulation study in Section 3.3 were considered in the experiments. The regression curve for the total tension loss rate at the early damage stage shown in Fig. 13 was used to estimate the total bolt torque loss rate. The error was calculated as 6.4% using Eq. (8), validating the effectiveness of the proposed TRS method for total damage severity estimation.

4.3 Results for local damage detection

Experiments were also carried out for 96 damage cases introduced in Section 3.3. The DI_{ji} was calculated for each pitch-catch test and compared with the simulated results as shown in Fig. 23. An excellent linear regression relationship between the simulation and experiment results was obtained as $y = 1.02x$ ($R^2 = 0.97$), which provides the basis of using the BPNN trained by the simulation dataset (using the tension losses) to estimate the local damage severity (in torque losses) on the experimental data. The damage indices of the 96 test samples were imported into the trained BPNN in Section 3.3 to estimate local damage severity with the results shown in Fig. 24. It has been found that most of the damages can be well estimated, though more false alarming cases occurred than in the simulation study. The estimated errors as well as the P, R, and F values for each row were shown in Table 3. The average local damage severity estimation error was 17.3%, and the average F value was 81.2%. The average false alarming rate (1-P) was 18%, whereas the average damage missing rate (1-R) was 17%.

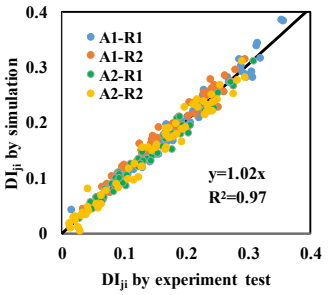

Fig. 23 Comparison of DI_{ji} between simulations and experiments

Table 3 Experimental local damage detection results

Row	P	R	F	$Error^{local}$
Row 1	0.854	0.804	0.828	0.161
Row 2	0.729	0.875	0.795	0.174
Row 3	0.729	0.946	0.824	0.171
Row 4	0.958	0.687	0.800	0.185
Average	0.818	0.828	0.812	0.173

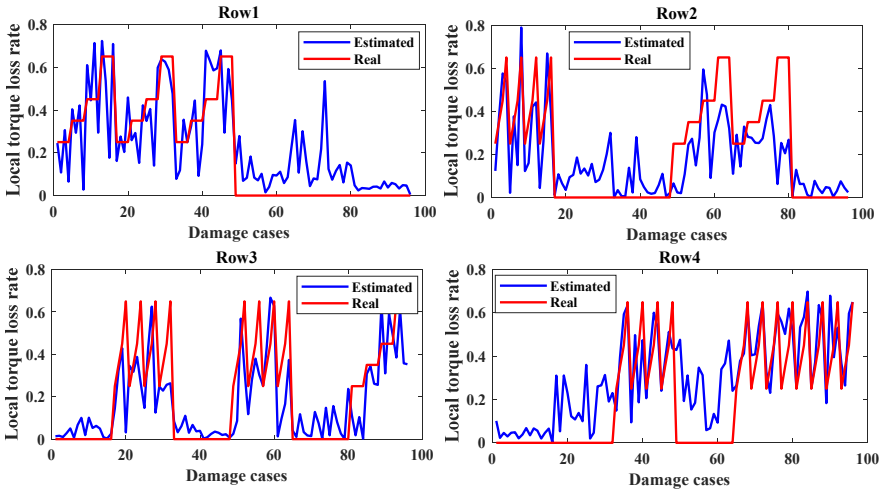

Fig. 24 Local damage severity estimation results by experiment tests

The errors in the experimental results were slightly larger than those in the simulation analysis, which may have come from the errors in the FEM simulation analysis to evaluate the damage index for each pitch-catch test (DI_{ji}) and the uncertainties in the test process. More efforts are needed for the FE model updating for the wave propagation analysis on the joint structure and the selection of the time reversed point (t_0) in TRS.

5. Conclusions

This study presented a TRS-BPNN-based method for bolt looseness detection and localization using guided SH wave generated by MS transducers. A small number (two pairs) of MS transducers were arranged in a pitch-catch mode, and the damage conditions were analyzed using the reconstructed signals excited by TRS. Wave path-dependent damage indices were proposed as the ratios of peak amplitudes of the reconstructed signals under the intact and damaged conditions for total damage severity (bolt looseness) estimation. BPNN was constructed to predict the damage locations and local damage severities using the damage indices from several wave propagation paths in the pitch-catch tests. From the numerical and experimental studies on the joint connected by multiple bolts, the following conclusions have been drawn:

(1) The total damage severity can be well estimated using the TRS-based method. The results are found to be robust under the influence of the external force and measurement noise. The regression curve between the overall damage index ($DI_{overall}$) and the total tension loss rate obtained from the simulation can be effectively used to evaluate the total damage severities for experimental data with a relative error of 6.4%, which is better than the wave energy method.

(2) The regression relationship between the wave path-dependent damage indices (DI_{ji}) from the simulation and experiment has been found to be excellent with $y = 1.02x$ and $R^2 = 0.97$, which provides the basis for using the BPNN trained by the simulation data for the experimental cases.

(3) Damage localization and local damage severity estimation for a joint with multiple bolts have been successfully conducted using a four-layered BPNN. The average damage localization accuracy (F value) in the simulation results was 92.4% with the average error of 12.6% for the local torque loss rate estimation. The BPNN trained using the simulation patterns was found to be very effective for predicting the local damages in the experimental cases with an average accuracy of 81.2% and error of 17.3%.

For the applications of the SH typed guided wave technique in the SHM of bolt-connected lap joints, future studies may address the following subjects: (1) FE model updating for the wave propagation analysis; (2) more specific local damage detection by increasing numbers of the transducers and input neuron nodes; (3) optimal transducer locations; and (4) environmental effects such as temperature.

Acknowledgments

The authors acknowledge the supports from the National Key R&D Program of China (2018YFE0125400, 2019YFE0112600) and National Natural Science Foundation of China (Grant Nos. 52078459, U1709216).

References

Ahmadian, H. and Jalali, H. (2007), "Identification of bolted lap joints parameters in assembled structures", *Mech. Syst. Signal Process.*, **21**(2), 1041-1050. https://doi.org/10.1016/j.ymssp.2005.08.015

Amerini, F. and Meo, M. (2010), "Structural health monitoring of bolted joints using linear and nonlinear acoustic/ultrasound methods", *Struct. Health Monitor.*, **10**(6), 659-672. https://doi.org/10.1177/1475921710395810

Baghalian, A., Senyurek, V.Y., Tashakori, S., McDaniel, D. and

Tansel, I.N. (2018), "A novel nonlinear acoustic health monitoring approach for detecting loose bolts", *J. Nondestr. Eval.*, **37**(2), 24. https://doi.org/10.1007/s10921-018-0478-0

Beena, K., Shruti, S., Sandeep, S. and Naveen, K. (2017), "Monitoring degradation in concrete filled steel tubular sections using guided waves", *Smart Struct. Syst., Int. J.*, **19**(4), 371-382. https://doi.org/10.12989/sss.2017.19.4.371

Biwa, S., Nakajima, S. and Ohno, N. (2004), "On the acoustic nonlinearity of solid-solid contact with pressure-dependent interface stiffness", *J. Appl. Mech.-Transact. ASME*, **71**(4), 508-515. https://doi.org/10.1115/1.1767169

Caccese, V., Mewer, R. and Vel, S.S. (2004), "Detection of bolt load loss in hybrid composite/metal bolted connections", *Eng. Struct.*, **26**(7), 895-906. https://doi.org/10.1016/j.engstruct.2004.02.008

Cha, Y.J., You, K. and Choi, W. (2016), "Vision-based detection of loosened bolts using the Hough transform and support vector machines", *Automat. Constr.*, **71**, 181-188. https://doi.org/10.1016/j.autcon.2016.06.008

Chen, D.D, Huo, L.S. and Song, G.B. (2020), "EMI based multi-bolt looseness detection using series parallel multi-sensing technique", *Smart Struct. Syst., Int. J.*, **25**(4), 423-432. https://doi.org/10.12989/sss.2020.25.4.423

Chung, J. and Sohn, H. (2020), "Detection and quantification of bolt loosening using RGB-D camera and mask R-CNN", *Smart Struct. Syst., Int. J.*, **27**(5), 783-793. https://doi.org/10.12989/sss.2021.27.5.783

Drenick, R.F., Wang, P.C., Yun, C.B. and Philappacopoulos, A.J. (1980), "Critical seismic response of nuclear reactors", *Nuclear Eng. Des.*, **58**(3), 425-435.

Fan, Z. and Lowe, M.J.S. (2009), "Elastic waves guided by a welded joint in a plate", *Proceedings of the Royal Society A-Mathematical Physical & Engineering Sciences*, **465**(2107), 2053-2068. https://doi.org/10.1098/rspa.2009.0010

Fasel, T.R., Kennel, M.B., Todd, M.D., Clayton, E.H. and Park, G. (2009), "Damage state evaluation of experimental and simulated bolted joints using chaotic ultrasonic waves", *Smart Struct. Syst., Int. J.*, **5**(4), 329-344. https://doi.org/10.12989/sss.2009.5.4.329

Fink, M., Cassereau, D., Derode, A., Prada, C., Roux, P., Tanter, M., Thomas, J.L. and Wu, F. (2000), "Time-reversed acoustic", *Reports on Progress Phys.*, **63**(12), 1933-1995. https://doi.org/10.1088/0034-4885/63/12/202

GB 50205 (2020), *Standard for acceptance of construction quality of steel structures*, China Planning Press, Beijing.

Gianesini, B.M., Cortez, N.E., Antunes, R.A. and Vieira, J. (2020), "Method for removing temperature effect in impedance-based structural health monitoring systems using polynomial regression", *Struct. Health Monitor.*, **20**(1), 202-218. https://doi.org/10.1177/1475921720917126

Hayashi, T. and Murase, M. (2005), "Defect imaging with guided waves in a pipe", *J. Acoust. Soc. Am.*, **117**(4), 2134-2140. https://doi.org/10.1121/1.1862572

Huda, F., Kajiwara, I., Hosoya, N. and Kawamura, S. (2013), "Bolt loosening analysis and diagnosis by non-contact laser excitation vibration tests", *Mech. Syst. Signal Process.*, **40**(2), 589-604. https://doi.org/10.1016/j.ymssp.2013.05.023

Hush, D.R. and Horne, B.G. (1993), "Progress in supervised neural networks", *IEEE Signal Process. Magaz.*, **10**(1), 8-39. https://doi.org/10.1109/79.180705

Jhang, K.Y., Quan, H.H., Ha, J. and Kim, N.Y. (2006), "Estimation of clamping force in high-tension bolts through ultrasonic velocity measurement", *Ultrasonics*, **44**, e1339-e1342. https://doi.org/10.1016/j.ultras.2006.05.190

Kamas, T., Poddar, B., Lin, B. and Yu, L.Y. (2015), "Assessment of temperature effect in structural health monitoring with piezoelectric wafer active sensors", *Smart Struct. Syst., Int. J.*, **16**(5), 835-851. https://doi.org/10.12989/sss.2015.16.5.835

Kubrusly, A.C. and Dixon, S. (2021), "Application of the reciprocity principle to evaluation of mode-converted scattered shear horizontal (SH) wavefields in tapered thinning plates", *Ultrasonics*, **117**, 106544. https://doi.org/10.1016/j.ultras.2021.106544

Liang, C., Sun, F.P. and Rogers, C.A. (1997), "Coupled electro-mechanical analysis of adaptive material systems determination of the actuator power consumption and system energy transfer", *J. Intell. Mater. Syst. Struct.*, **5**(1), 12-20. https://doi.org/10.1177/1045389X9700800406

Lopes, V., Park, G., Cudney, H.H. and Inman, D.J. (2000), "Impedance-based structural health monitoring with artificial neural networks", *J. Intell. Mater. Syst. Struct.*, **11**(3), 206-214. https://doi.org/10.1106/H0EV-7PWM-QYHW-E7VF

Miao, H.C. and Li, F.X. (2021), "Shear horizontal wave transducers for structural health monitoring and nondestructive testing: A review", *Ultrasonics*, **114**, 106355. https://doi.org/10.1016/j.ultras.2021.106355

Min, J., Park, S., Yun, C.B., Lee, C.G. and Lee, C. (2012), "Impedance-based structural health monitoring incorporating neural network technique for identification of damage type and severity", *Eng. Struct.*, **39**, 210-220. https://doi.org/10.1016/j.engstruct.2012.01.012

Moustakidis, S., Kappatos, V., Karlsson, P., Selcuk, C., Gan, T.H. and Hrissagis, K. (2014), "An intelligent methodology for railways monitoring using ultrasonic guided waves", *J. Nondestr. Eval.*, **33**(4), 694-710. https://doi.org/10.1007/s10921-014-0264-6

Na, S. and Lee, H.K. (2012), "Resonant frequency range utilized electro-mechanical impedance method for damage detection performance enhancement on composite structures", *Compos. Struct.*, **94**(8), 2383-2389. https://doi.org/10.1016/j.compstruct.2012.02.022

Nikravesh, S.M.Y. and Goudarzi, M. (2017), "A review paper on looseness detection methods in bolted structures", *Latin Am. J. Solids Struct.*, **14**(12), 2153-2176. https://doi.org/10.1590/1679-78254231

Pai, N.G. and Hess, D.P. (2002), "Experimental study of loosening of threaded fasteners due to dynamic shear loads", *J. Sound Vib.*, **253**(3), 585-602. https://doi.org/10.1006/jsvi.2001.4006

Park, S., Yun, C.B., Roh, Y. and Lee, J.J. (2005), "Health monitoring of steel structures using impedance of thickness modes at PZT patches", *Smart Struct. Syst., Int. J.*, **1**(4), 339-353. https://doi.org/10.12989/sss.2005.1.4.339

Park, S., Yun, C.B., Roh, Y. and Lee, J.J. (2006), "PZT-based active damage detection techniques for steel bridge components", *Smart Mater. Struct.*, **15**(4), 957-966. https://doi.org/10.1088/0964-1726/15/4/009

Parvasi, S.M., Ho, S.C.M., Kong, Q.Z., Mousavi, R. and Song, G.B. (2016), "Real time bolt preload monitoring using piezoceramic transducers and time reversal technique-A numerical study with experimental verification", *Smart Mater. Struct.*, **25**(8), 085015. https://doi.org/10.1088/0964-1726/25/8/085015

Pnevmatikos, N.G., Blachowski, B., Hatzigeorgiou, G.D. and Swiercz, A. (2016), "Wavelet analysis based damage localization in steel frames with bolted connections", *Smart Struct. Syst., Int. J.*, **18**(6), 1189-1202. https://doi.org/10.12989/sss.2016.18.6.1189

Razi, P., Esmaeel, R.A. and Taheri, F. (2013), "Improvement of a vibration-based damage detection approach for health monitoring of bolted flange joints in pipelines", *Struct. Health Monitor.*, **12**(3), 207-224. https://doi.org/10.1177/14759217134796

Su, Z.Q., Ye, L. and Lu, Y. (2006), "Guided Lamb waves for identification of damage in composite structures: A review", *J.*

Sound Vib., **295**(3-5), 753-780. https://doi.org/10.1016/j.jsv.2006.01.020

Tang, Z.F., Sui, X.D., Duan, Y.F., Zhang, P.F. and Yun, C.B. (2021), "Guided wave-based cable damage detection using wave energy transmission and reflection", *Struct. Control Health Monitor*., **28**(5), e2688. https://doi.org/10.1002/stc.2688

Yang, J., Liu, P., Yang, S., Lee, H. and Sohn, H. (2015), "Laser based impedance measurement for pipe corrosion and bolt-loosening detection", *Smart Struct. Syst*., *Int. J*., **15**(1), 41-55. https://doi.org/10.12989/sss.2015.15.1.041

Zhang, Z., Xu, H., Liao, Y., Su, Z. and Xiao, Y. (2017), "Vibro-acoustic modulation (VAM)-inspired structural integrity monitoring and its applications to bolted composite joints", *Compos. Struct*., **176**, 505-515. https://doi.org/10.1016/j.compstruct.2017.05.043

Zhang, Y., Li, D.S. and Zheng, X.T. (2019), "Detection and location of bolt group looseness using ultrasonic guided wave", *Smart Struct. Syst*., *Int. J*., **24**(3), 293-301. https://doi.org/10.12989/sss.2019.24.3.293

Zhang, M.R., Tang, Z.F., Yun, C.B., Sui, X.D., Chen, J. and Duan, Y.F. (2021), "Bolt looseness detection using SH guided wave and wave energy transmission", *Smart Mater. Struct*., **30**(10), 105015. https://doi.org/10.1088/1361-665X/ac1d90

Zhou, Z.H. (2016), *Machine Learning*, Tsinghua University Press, China, Beijing.

HJ